Development And Characterization of Green Synthesized Silver Nanoparticles of Anticancer Activity

Amrita Gupta, Dr. Sameer Rastogi*

HIMT College of Pharmacy – Greater Noida, 201301, Uttar Pradesh, India

Abstract

Objective: The aim of this study is to develop and characterize silver nanoparticles (AgNPs) using turmeric extract through a green synthesis method. These AgNPs will be investigated for their potential as a delivery system for anticancer drugs targeted to lung cancer cells.

Method: AgNPs were synthesized using turmeric extract, and their surface was functionalized by conjugating hyaluronic acid as a ligand. The cytotoxicity of these AgNPs towards lung cancer cells was evaluated. To characterize the AgNPs, a comprehensive analysis was conducted using techniques such as ultraviolet-visible absorption spectroscopy, Fourier transform infrared spectroscopy, scanning electron microscopy, differential scanning calorimetry, X-ray diffraction, and selected area electron diffraction.

Results: The synthesized AgNPs formulation exhibited a spherical shape, as confirmed by SEM analysis. The optimal particle size was determined to be 279.9 nm when using a silver nitrate concentration of 1 mM. Furthermore, the optimized formulation demonstrated a high entrapment efficiency of 92.5±1.2%. In vitro drug release studies demonstrated a sustained release profile, enabling a gradual and prolonged release of the drug. The formulation also exhibited better stability at 4 ± 2°C compared to 28 ± 2°C. Ex vivo studies were conducted on a lung cancer cell line (NCIH226), and the HA/PTX/AgNPs formulation displayed superior inhibition of cell growth compared to other formulations, including PTX/AgNPs and Free PTX.

Conclusion: The conjugation of hyaluronic acid as a ligand significantly enhanced the effectiveness of the AgNPs formulation of PTX (paclitaxel). This improved efficacy can be attributed to the utilization of hyaluronic acid receptor-mediated endocytosis, which enhances the uptake and intracellular delivery of the nanoparticles. Furthermore, the formulations exhibited sustained release properties and remained stable at a temperature of 4 ± 2°C.

Keywords: Anti-cancer drug; Lung Cancer, cell cytotoxicity; Sustained release; Targeted drug delivery

Introduction

Cancer development is primarily driven by genetic mutations or abnormal activation of cellular genes known as oncogenes, which regulate cell growth and mitosis. Extensive research has identified around 100 oncogenes involved in cancer progression. Conversely, anti-oncogenes act as protective mechanisms, suppressing the activation of specific oncogenes. Disruption of this balance through loss or inactivation of anti-oncogenes can lead to oncogene activation and promote cancer onset. Most mutated cells are regulated by feedback mechanisms that limit cancer development, leaving only a minority of cells to become cancerous. The immune system plays a vital role in eliminating potentially cancerous cells, producing antibodies or sensitized lymphocytes to attack and eliminate them. Suppressed immune systems, such as in organ transplant recipients receiving immunosuppressant drugs, increase the risk of cancer development, emphasizing the importance of immune surveillance (Hanahan , 2022; Blackadar) 2016 .

Lung cancer is the second most common malignancy and a major cause of cancer-related deaths in both males and females. While smoking accounts for about 80% of lung cancers, non-smokers also face a significant burden of the disease. Causes of lung cancer include asbestos, radon, heavy metals, radiation exposure, air pollution, and genetic factors. Treatment approaches for lung cancer include surgical removal of the tumor, chemotherapy, radiation therapy, or a combination of these modalities. Adjuvant therapy may follow surgical resection, while targeted therapy focuses on specific molecular targets involved in cancer growth and progression, improving treatment efficacy with minimal harm to healthy cells (Islami et al., 2018; Cruz et al., 2011).

Targeted drug delivery aims to enhance therapeutic agent accumulation within tumors or diseased tissues while minimizing distribution to healthy tissues. Nanoparticles, liposomes, or drug conjugates are utilized in this approach to selectively deliver drugs to the intended target site, maximizing efficacy and reducing side effects. Among the nanoparticles used for targeted drug delivery, silver nitrate nanoparticles have gained attention due to their unique properties, including cytotoxicity against cancer cells, the ability to be functionalized with targeting ligands, photothermal properties, and enhanced imaging capabilities (Rajendran et al., 2023; Ezhilarasan et al., 2022).

Hyaluronic acid (HA) has emerged as a promising ligand in lung cancer due to its specific targeting of receptors overexpressed on lung cancer cells, such as CD44. Conjugating HA to nanoparticles or drug carriers enables targeted drug delivery to the tumor site. HA's high biocompatibility and biodegradability further contribute to its applicability (Prajapati et al., 2019). Additionally, HA has shown potential in inhibiting lung cancer cell proliferation and metastasis, making HA-based targeted therapies promising for improving lung cancer treatment outcomes (Luo et al., 2016). Further research is needed to optimize HA-based ligand-targeted strategies for lung cancer. Paclitaxel, a drug that stabilizes microtubules and inhibits cell division, is commonly used in combination with other chemotherapy agents for advanced or metastatic lung cancer.

Formulation and Characterization

Materials Required

Hyaluronic acid was procured from the Otto Chemie Pvt Ltd, Mumbai Silver nitrate was procured from CDH Pvt. Ltd. New Delhi. Ethano and distilled water and other solvent s were of analytical grade.

Extract Preparation

In order to obtain the extract of turmeric powder, a precise measurement of 6.8 grams of turmeric powder was carefully weighed and combined with 100mL of distilled water. Subsequently, the mixture underwent a 12-minute boiling process, followed by a cooling period of 15 minutes at room temperature. To ensure clarity and purity, the extract was then meticulously filtered using filter paper and subjected to centrifugation at 1000 RPM for 10 minutes at a temperature of 25ºC.

Green Synthesis of silver nanoparticles

The synthesis of silver nanoparticles (AgNPs) was accomplished by employing a previously reported technique, which was suitably modified for the purpose. To facilitate the reduction of silver ions, 4 mL of extract was subjected to moderate stirring at room temperature while being treated with 16 mL of aqueous solution containing varying concentrations of $AgNO_3$ (1 mM, 1.5 mM, and 2 mM). The stirring process continued overnight until the complete synthesis of AgNPs was achieved. Initially, upon the addition of the extract, the solution exhibited a yellow color, indicating the presence of precursor components. However, because of the sustained moderate stirring during the overnight period, the color of the solution underwent a transformation, evolving into a rich, dark shade, indicative of the successful formation of AgNPs. Drug PTX was loaded by adding 5 mg/mL of PTX at a final volume of prepared

AgNPs. The solution then kept for stirring overnight centrifuged to removed unbounded drug (Alsammarraie et al., 2018).

HA Conjugation on AgNPs

A solution containing 100 mg of hyaluronic acid (HA) was dissolved in water with a pH of 8.0. To activate the HA, N-hydroxysuccinimide (NHS) and EDC.HCl were added at concentrations of 0.50 mM each. The mixture was allowed to react for 6 hours. The NHS acts as a catalyst, while EDC.HCl functions as a coupling agent, facilitating the formation of amide bonds. The activated HA was then added to an aqueous suspension of AgNPs. The reaction mixture was continuously stirred for an additional 6 hours for effective binding. Subsequently, dialysis process was carried out for 24 hours using deionized (DI) water as the dialysis medium. Dialysis was performed using a membrane with a molecular weight cut-off of 3500 KDa. Dialysis helps in removing small molecules and impurities while retaining the larger HA-AgNP complex (Ferreres et al., 2021).

Characterization of AgNPs

FTIR Analysis

FTIR analysis was conducted on PTX, HA, and AgNPs using a Bruker Fourier transform infrared (FT-IR) spectrometer. The samples were placed and their spectra were recorded. After analyzing each sample, the FTIR device was cleaned using a mixture of alcohol and water before proceeding to analyze the next sample.

Particle size and Polydispersity index

The size of AgNPs was evaluated using a Malvern Zetasizer, a laser Doppler anemometry instrument that employs laser-based multiple angle particle electrophoresis. This method determines the distribution of mobility and the size of particles in liquid suspensions. The polydispersity index serves as a dimensionless metric to quantify the extent of size variation in NPs and can be utilized to assess the dispersibility of the system. A monodispersed colloidal dispersion exhibits a polydispersity index (PDI) of zero. Conversely, colloidal dispersions containing particles with a PDI of approximately 0.05 are regarded as monodispersed, while those with a PDI exceeding 0.5 are assumed to possess a wide range of particle sizes (Rajput et al., 2020; Haque et al., 2017).

Scanning electron microscope (SEM)

The AgNPs were subjected to a vacuum-drying process, followed by a comprehensive morphological analysis utilizing the Carl Zeiss Supra 55 electron microscope model. To generate thin films of the sample, a minute amount was delicately dispensed onto a carbon-

coated copper grid, with excess solution promptly eliminated using blotting paper. Subsequently, the films on the SEM grid were dried under the illuminating influence of a mercury lamp for a duration of 5 minutes (Goudarzi et al., 2016).

Differential scanning Colorimetry (DSC) study

The crystal form of PTX, HA, and AgNPs was determined using DSC analysis on a Rigaku SmartLab Cu 1.5 KV instrument. The samples were heated from 40 to 400°C at a rate of 5°C/minute under a nitrogen purged, inert atmosphere, with a blank pan as reference.

X-Ray Diffraction (XRD) Study

On termination of the combination of nanoparticles, the receptivity combination became centrifugation at 8000 rpm for 10 min additionally the nano particle modified into subtle in germ free diffused water and cleaned 3 times thereby suggests that of centrifugation to evacuate polluting impacts. 1 ml of the nano particle solution on a pitcher slide and dried at 40°C in an oven. Thin film changed into acquired by way of way of repeating the way 3-four times. The crystalline shape of bio-decreased metal silver NPs becomes affirmed through using XRD.

Estimation of drug entrapment

A 10 mg nanoparticle sample was dissolved in 50 ml of PBS at pH 7.4. The suspension underwent ultra-centrifugation at 1500 rpm for 15 min. The resulting supernatant was analyzed for PTX at 240 nm. The loading capacity and entrapment efficiency of each nanoparticle were calculated using the following formulas:

$$\%EE = \frac{\text{Wt.of PTX in NPs} - \text{Wt.PTX in Supernatent}}{\text{Wt. of PTX in NPs}} \times 100$$

In vitro drug release study

The release of the drug PTX was evaluated through in-vitro experiments using AgNPs. The drug release tests were conducted for a duration of 72 hours in a PBS solution with varying pH levels of 7.4 and 5.3. To perform the tests, a nanoparticle formulation containing 5 mg/ml of PTX was placed inside a dialysis bag. This bag was then suspended in 50 ml of Phosphate buffer solution (PBS) at a temperature of 37°C, and gentle magnetic stirring at 100 rpm was applied. At specified time intervals, 2 ml of the buffer liquid was taken out and replaced with fresh PBS. The amount of PTX released at each time interval was determined using UV-Spectrophotometry at a wavelength of 240 nm, employing a UV-1601 PC Shimadzu Spectrophotometer from Japan (Gomes et al., 2021).

Ex-Vivo study

MTT [(3-(4,5-dimethylthiazol-2-yl)-2,5-diphenyl tetrazolium bromide)] is a pale yellow substrate that is cleaved by living cells to yield a dark blue formazan product. This process requires active mitochondria, and even freshly dead cells do not cleave significant amount of MTT. Thus, the amount of MTT cleaved is directly proportional to the number of viable cells present, which is quantified by colorimetric methods. This assay was performed at Deshpande Laboratories, Bhopal using the standard operating procedures. Briefly the compounds were dissolved in DMSO and serially diluted with complete medium to get the concentrations a range of test concentration. DMSO concentration was kept < 0.1% in all the samples NCIH 226 maintained in appropriate conditions were seeded in 96 well plates and treated with different concentrations of the test samples and incubated at 37 °C, 5% CO_2 for 96 hours. MTT reagent was added to the wells and incubated for 4 hours; the dark blue formazan product formed by the cells was dissolved in DMSO under a safety cabinet and read at 550nm. Percentage inhibitions were calculated and plotted with the concentrations used to calculate the IC50 values (Desai et al., 2023; Ashique et al., 2023).

Stability studies:

Two formulations, AG/PTX NPs and HA/AG/PTX NPs, were tested for stability. The formulations were stored under two different conditions: 4±2°C and 25±2°C. Screw-capped, amber-colored glass bottles were used to store the formulations. The samples were analyzed at intervals of 30, 60, and 90 days to assess changes in residual drug content. The purpose of this testing was to evaluate the stability of the formulations over an extended period of time under different storage conditions.

Results and discussion

The AgNP formulation was optimized to maximize drug entrapment efficiency. Three different formulations were created, each with different concentrations of silver nitrate: 1 mM, 1.5 mM, and 2.0 mM. Further investigation was conducted to understand the properties of the prepared formulation. This included SEM analysis to examine the shape and surface morphology of the particles. Additionally, XRD, DSC, and particle size studies were performed to gain more insights into the formulation.

UV-Vis Absorption Spectrum

The UV-Vis spectra presented in Figure 1 depict the absorption patterns of nanoparticles (NPs) at varying concentrations of $AgNO_3$. Initially, no evident absorption peak was observed in any

of the solutions. However, after 3 hours, a small absorption peak began to form. Subsequently, the highest absorption peak was detected after 24 hours in the solution with a concentration of 1.5 mM. This peak exhibited an intense band at 420 nm, resulting from the combined contribution of turmeric extract absorbance and surface plasmon resonance generated by the collective oscillations of conducting electrons in the silver NPs. As time progressed, the color of the solution gradually darkened, indicating continuous formation of AgNPs. This was further supported by the increasing maximum absorption values observed in all solutions over time.

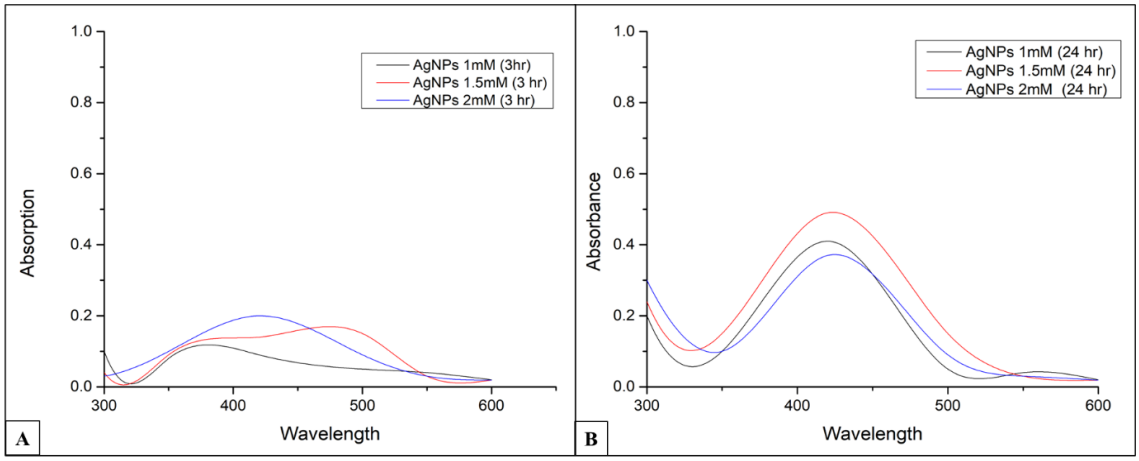

Figure *1*: The UV-Vis Spectrum Graphs of silver nitrate solution and with Different Ratios at Reaction Time (a) 24 hours, (b) 48 hours, (c) 96 hours

FTIR

The FTIR data for the hyaluronic acid polymer and Developed NPs reveals important information about its molecular structure and functional groups (Figure 2). Several peaks were observed at specific wavenumbers, indicating distinct vibrations and bonds present in the polymer. Two peaks were identified at 3567.61 cm^{-1} and 3397.62 cm^{-1}, representing the stretching vibrations of hydroxyl (O-H) groups. These hydroxyl groups are a characteristic feature of hyaluronic acid, contributing to its hydrophilic nature and potential interactions with water molecules. Another significant peak was observed at 2557.84 cm^{-1}, corresponding to the Amide A band. This peak is associated with the stretching vibration of N-H groups, indicating the presence of amide bonds within the polymer structure. Amide bonds play a crucial role in forming the backbone of hyaluronic acid, providing stability and contributing to its biocompatibility. A peak at 1699.71 cm^{-1} indicated the stretching vibration of carbonyl (C=O) groups, suggesting the presence of carbonyl functional groups such as esters or acids in the polymer. These carbonyl groups can influence the reactivity and chemical properties of hyaluronic acid, enabling various modifications and cross-linking strategies. Symmetric and

asymmetric stretching vibrations of carboxylate (COO-) groups were identified by peaks at 1451.63 cm^{-1} and 1398.7 cm^{-1}, respectively. Carboxylate groups are integral to hyaluronic acid's structure and function, contributing to its anionic nature and potential interactions with positively charged molecules or surfaces. Additionally, a peak at 1252.46 cm^{-1} indicated the C-O stretching vibration of carboxylate groups, further confirming their presence in the polymer. These carboxylate groups play a crucial role in the overall charge and solubility of hyaluronic acid, influencing its behavior in various applications. The peak at 1097.88 cm^{-1} represented the C-O stretching vibration of glycosidic bonds. This peak indicates the presence of glycosidic linkages, which are characteristic of hyaluronic acid's polysaccharide structure (Figure 8) (Giubertoni et al., 2019).

The FTIR data of formulation is represented in Figure 9. At 3420.73 cm^{-1}, a peak is observed indicating the presence of stretching vibrations of hydroxyl (OH) groups. Another peak appears at 2923.02 cm^{-1}, corresponding to the stretching vibrations of methylene (CH_2) groups. This peak indicates the presence of aliphatic chains or saturated hydrocarbons in the formulation. The peak observed at 1797.12 cm^{-1} suggests the presence of carbonyl (C=O) groups. This indicates the presence of ester, ketone, or carboxylic acid functional groups in the formulation. A peak at 1509.96 cm^{-1} corresponds to the stretching vibrations of aromatic C=C bonds, indicating the presence of aromatic rings in the formulation. At 1391.71 cm^{-1}, another peak is observed, suggesting the presence of carboxylic acid (COOH) groups. A peak at 1229.03 cm^{-1} corresponds to the stretching vibrations of C-N bonds, indicating the presence of amine groups in the formulation (Mavaei et al., 2020).

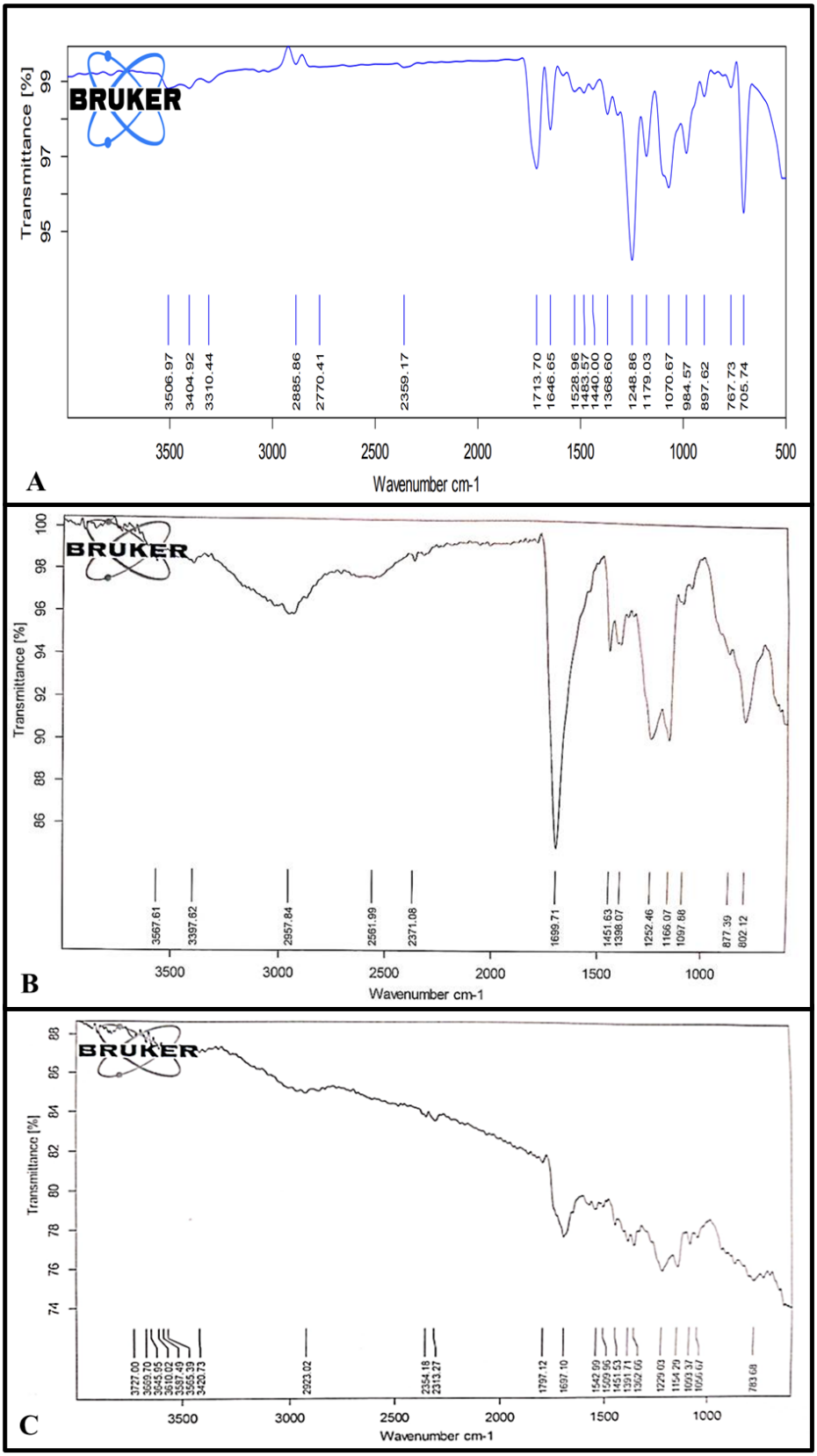

Figure 2: FTIR of (A) PTX, (B) Hyaluronic Acid (C) AgNPs

Particle Size and PDI

AgNPs were synthesized using Turmeric Extract as the precursor. The concentration of $AgNO_3$ in the NPs was varied in three different formulations: 1.0 mM, 1.5 mM, and 2.0 mM. The size of the NPs was measured (Figure 3), and the results showed that the sizes were 340.8 nm, 279.9 nm, and 743.1 nm for the respective concentrations. The polydispersity index (POI), a measure of the distribution of particle sizes, was determined and found to be 0.526, 0.698, and 0.801, respectively. Lastly, the percentage entrapment efficiency (%EE) of the drug in the NPs was evaluated, and the results showed values of 87.4±1.3%, 92.5±1.2%, and 91.6±1.7% for the three concentrations, respectively.

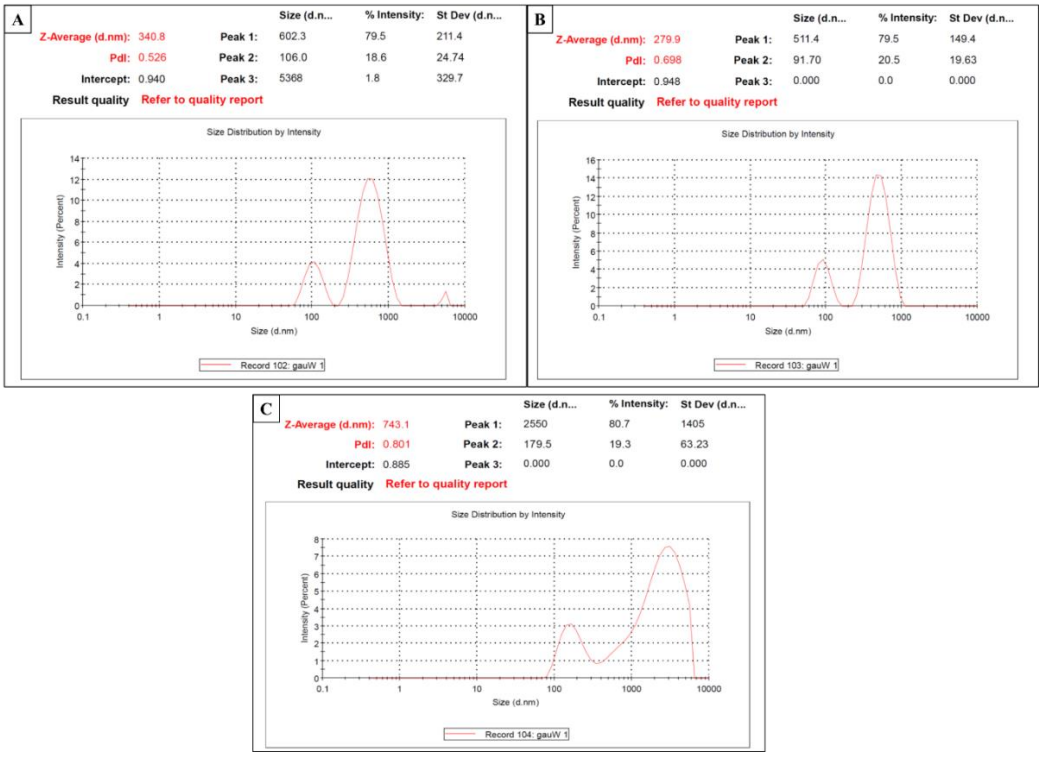

Figure*3*: Particle and PDI of AgNPs of three different concentration (A) 1.0 mM; (B) 1.5 mM; (C) 2.0 mM.

Scanning electron microscopy (SEM)

SEM is an methodology for elucidating the surface morphology of samples. By capturing the reflected electrons from the sample's surface, SEM enables the acquisition of high-resolution images that provide valuable insights into crucial nanoparticle attributes, including size, shape, topography, composition, and electrical conductivity. In the present investigation, the SEM analysis of silver nanoparticles synthesized using turmeric extract revealed the presence of nanoparticles exhibiting an oval and spherical morphology (Figure 4).

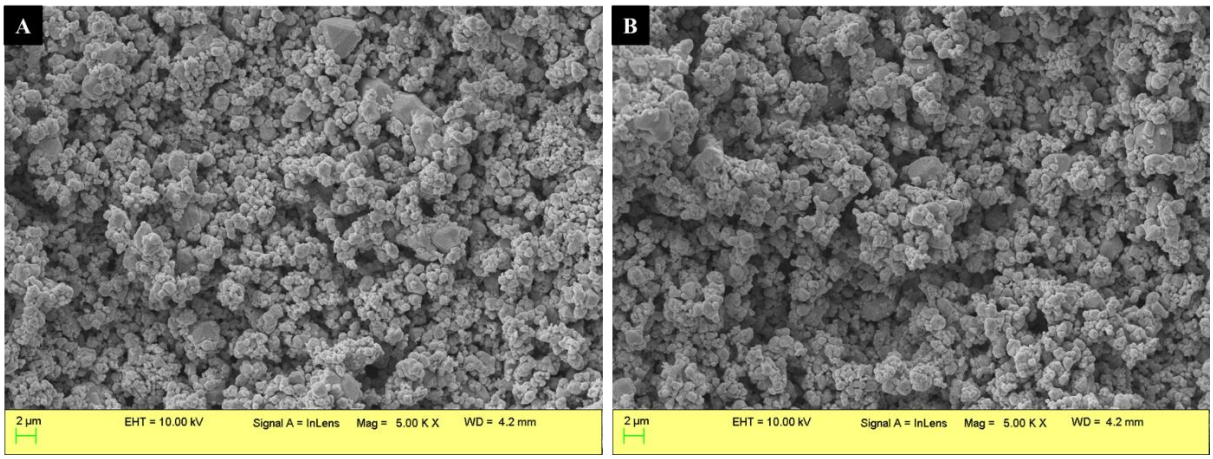

Figure 4: Scanning electron microscopy of (A) AgNPs and (B) HA/AgNPs

X-Ray difraction (XRD)

XRD is a tactic for the determination of crystallinity of AgNPs. When X-rays interact with the atoms on the crystal surface, the atoms arrange themselves at specific distances, forming a pattern of diffraction. In our study, AgNPs prepared using aqueous turmeric extract exhibited a crystalline structure. The XRD diffraction patterns of PTX and the AgNPs formulation were compare. It was observed that PTX indicated quite sharp crystalline peaks, indicating its molecular compound characteristics with some level of crystallinity d (Figure 5A). However, in the drug-loaded nanoparticles, the crystalline peaks were nearly absent, resembling the amorphous characteristics of the nanoparticles. This suggests that the drug was adsorbed on the nanoparticles and that the PTX within the nanoparticle matrix was either dispersed at a molecular level or in an amorphous form. The state of the drug incorporated in the nanoparticles is an important factor affecting the release behavior of the drug. Notably, there were no significant changes in the absorption peaks between the blank nanoparticles and the drug-loaded nanoparticles (Figure 5B). It is worth mentioning that the absorption peaks of the pure drug were not completely masked due to the adsorption of the drug on the surface of the nanoparticles.

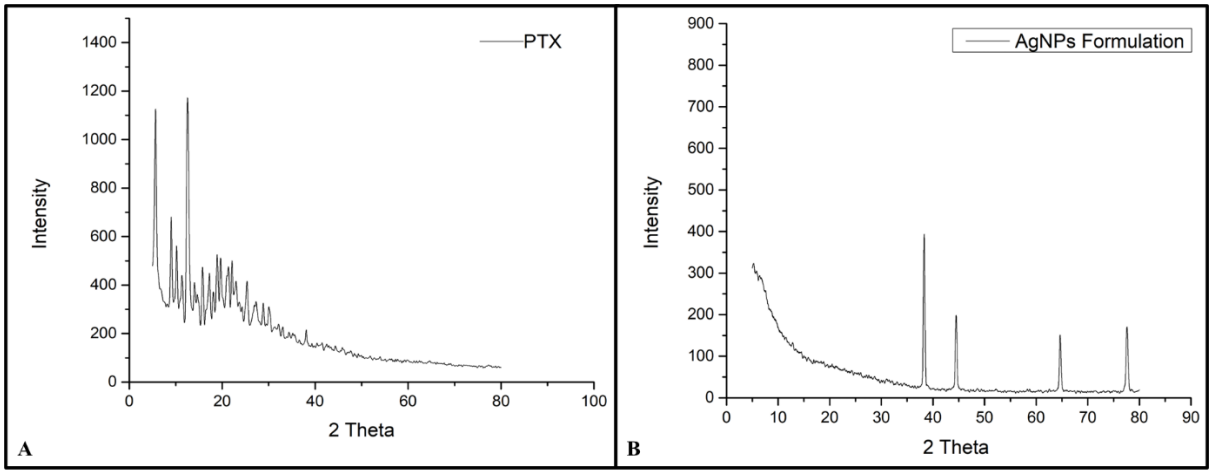

Figure 5: XRD spectra of (A) PTX (B) AgNPs

DSC Analysis

The examination of the thermal properties of NPs and the physicochemical state of drugs and drug combinations was greatly aided by the use of DSC analysis (Figure 6). DSC analysis measures the heat flow associated with physical and chemical changes in a substance as a function of temperature. The DSC Thermogram reveals peaks on the graph that represent different thermal events (Stino et al., 2022). At a temperature of 222.28°C, PTX exhibits an endothermic peak. This peak indicates that PTX underwent an endothermic reaction during this temperature range, specifically a process referred to as "melting." In other words, the drug absorbed heat energy from its surroundings, causing it to transition from a solid state to a liquid state. Similarly, HA displays an exothermic peak at 248.26°C. An exothermic peak suggests that HA experienced an exothermic reaction during this temperature range, which in this case, is attributed to crystallization. Crystallization is a process where a substance rearranges its molecular structure to form a solid crystal lattice, releasing heat energy in the process. As for AgNPs loaded with PTX, small exothermic peaks are observed at 257.25°C. These peaks indicate that there was a release of heat energy during this specific temperature range for AgNPs. However, the exothermic peaks for AgNPs are relatively smaller compared to the endothermic peak of PTX and the exothermic peak of HA, suggesting that the heat release during this temperature range for AgNPs is less significant. The DSC analysis of PTX, HA, and AgNPs loaded with PTX provided valuable qualitative and quantitative data about their thermal properties. The endothermic peak for PTX indicated its melting behavior, while the exothermic peak for HA indicated crystallization. The small exothermic peaks for AgNPs suggested some heat release, albeit to a lesser extent compared to PTX and HA. These findings

contribute to a better understanding of the physicochemical characteristics and behavior of these substances under thermal conditions.

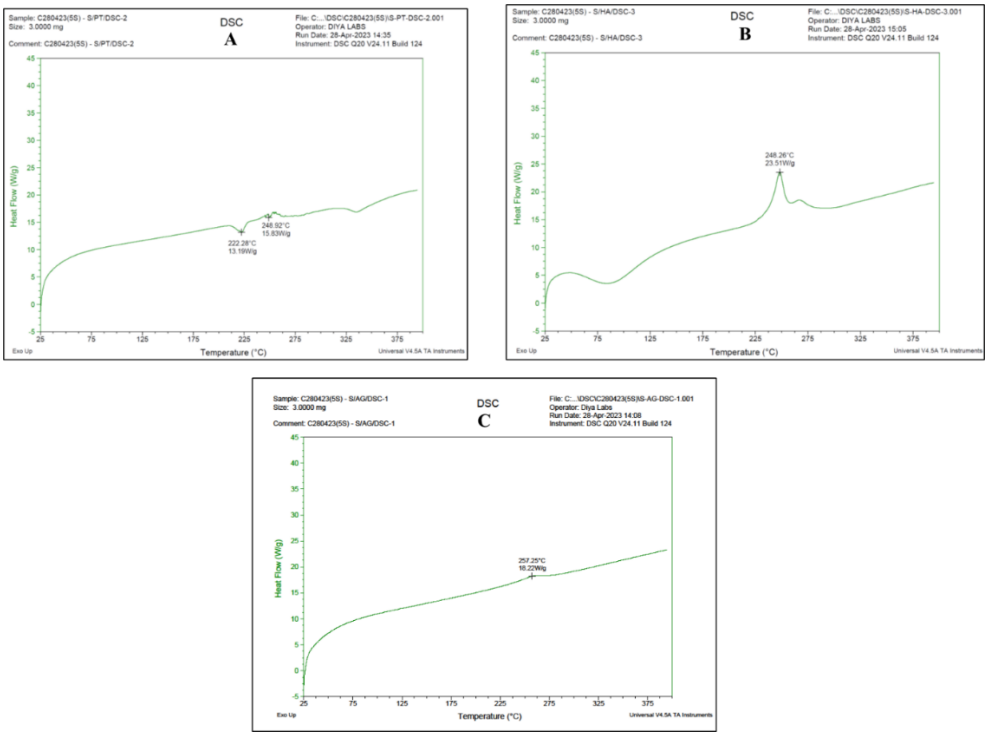

Figure 6: DSC thermograms of (A) PTX and (B) HA and (C) AgNPs

Entrapment Efficiency

The entrapment efficiency of the drug in these formulations was measured as a percentage. For the 1.0 mM formulation, the entrapment efficiency was determined to be 87.4±1.3%. The 1.5 mM formulation exhibited a higher entrapment efficiency of 92.5±1.2%. Similarly, the 2.0 mM formulation demonstrated an entrapment efficiency of 91.6±1.7%. These results suggest that increasing the concentration of $AgNO_3$ in the NPs leads to a slight improvement in the entrapment efficiency of the drug, and further increasing the concentration the entrapment efficiency found to be decreased.

Table 1: Particle size, Zeta potential, PDI and % Entrapment efficiency of AgNPs formulations.

Concentration of $AgNO_3$	1.0 mM	1.5mM	2.0mM
Size (nm)	340.8	279.9	743.1
PDI	0.526	0.698	0.801
%EE	87.4±1.3	92.5±1.2	91.6±1.7

Drug Release

The results of the in vitro drug release from the AgNPs formulation in phosphate buffer (pH 7.4) are presented in Figure 7. As time progressed, the release of the drug increased for all three formulations. After 72 hours, the PTX/AgNPs (pH 7.4) formulation exhibited the highest drug release at 99.0%, followed closely by the HA/PTX/AgNPs (pH 7.4) formulation at 96.7%. The PTX (pH 7.4) formulation showed a slightly lower drug release of 94.4% after 48 hours. These results indicate that the AgNPs formulations, particularly PTX/AgNPs (pH 7.4) and HA/PTX/AgNPs (pH 7.4), have a sustained release profile, allowing for a controlled and gradual release of the drug over an extended period of time (Figure 7A). Similarly, the in vitro drug release from different AgNPs formulations in phosphate buffer (pH 5.3) was evaluated over a period of time. The drug release profile varied depending on the formulation and time. Initially, at 0 hours, there was no drug release observed in any of the formulations. However, as the time progressed, the drug release increased. At 72 hours, the PTX/AGNPs formulation exhibited a drug release of 95.8%, while HA/PTX/AgNPs formulation showed a slightly lower release of 92.9%. Overall, the results indicate that the PTX/AgNPs formulation achieved a higher drug release compared to HA/PTX/AgNPs, suggesting its potential as a drug delivery system. At pH 5.3, the PTX/AgNPs and HA/PTX/AgNPs formulations demonstrated sustained drug release, with PTX/AgNPs exhibiting the highest release at 99.0% after 72 hours. At pH 5.3, PTX/AgNPs achieved a drug release of 95.8% after 72 hours, surpassing the release observed in HA/PTX/AgNPs (92.9%). These results highlight the potential of HA/PTX/AgNPs as an effective drug delivery system, particularly in tumor environments where sustained release is desired. Sustained effect at pH 5.3 and pH 7.4 could be due to the shielding potential of HA (Figure 7B).

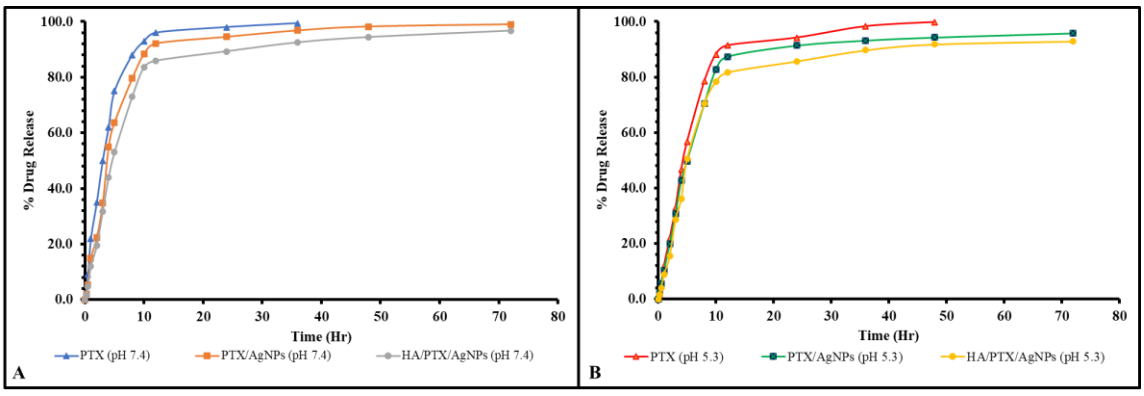

Figure 7. In vitro drug release from AgNPs at pH 7.4 and 5.3

Cell line Studies

The MTT assay was performed to assess the percentage of growth inhibition in NCIH226 cells

by the NP formulation at different concentrations. (Figure 8). At a concentration of 10, the cell viability ratios were 63.25, 66.52, and 68.15 for Free PTX, PTX/AgNPs and HA/PTX/AgNPs, respectively. As the concentration decreased, the cell viability ratios also decreased. For the concentration of 0.001, the cell viability ratios were 8.85, 6.34, and 8.41 for Free PTX, PTX/AgNPs and HA/PTX/AgNPs, respectively. The IC_{50} values, representing the concentration at which 50% inhibition was observed, were 0.7, 0.4, and 0.2 for Free PTX, PTX/AgNPs and HA/PTX/AgNPs, respectively. These results demonstrate the effect of varying concentrations on cell viability and provide insights into the inhibitory effects of the tested samples. The formulation with the lowest IC50 value is generally considered the most effective in terms of inhibiting cell viability. Comparing the IC50 values for the three formulations (Free PTX, PTX/AgNPs and HA/PTX/AgNPs), we can see that HA/PTX/AgNPs has the lowest IC_{50} value of 0.2. This suggests that HA/PTX/AgNPs formulation exhibits the highest potency in inhibiting cell viability among the tested concentrations. Therefore, based on the given information, the HA/PTX/AG NPs formulation appears to be the most effective formulation in terms of its inhibitory effect on cell viability.

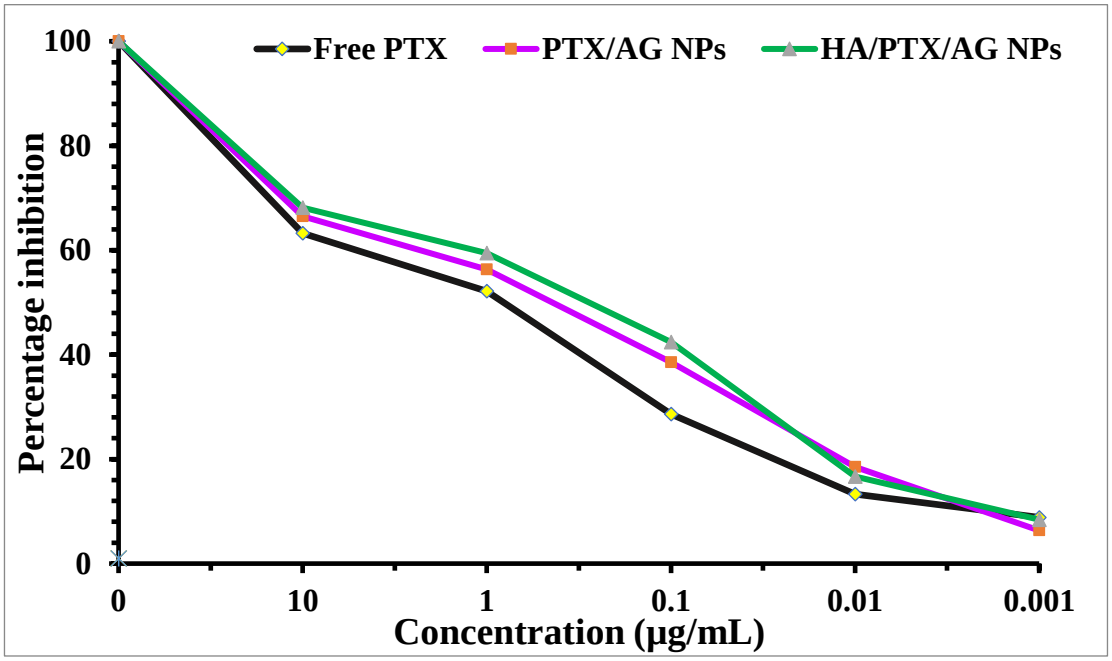

Figure 8: Percentage inhibition by AgNP formulations at different concentration

Stability Studies

The stability of two formulations, AG/PTX NPs and HA/AG/PTX NPs, was evaluated. The percentage of residual PTX content was determined by comparing it to the initial drug content, which was set at 100%. The results showed that when stored at 4±2°C (Figure 9A), the

AG/PTX NPs and HA/AG/PTX NPs formulations exhibited minimal degradation, with only 4-5% reduction in PTX content after 90 days, indicating high stability. However, when stored at 25±2°C, the formulations showed a decrease in residual drug content below 90% after 90 days (Figure 9B). These findings demonstrate that the nanotube formulations stored at lower temperatures (4±2°C) are more stable compared to those stored at higher temperatures (25±2°C). The reason for the higher stability of the formulations stored at 4±2°C can be attributed to the effect of temperature on chemical reactions and degradation processes. Lower temperatures generally slow down chemical reactions, reducing the rate of drug degradation. Additionally, temperature fluctuations and higher temperatures can promote the breakdown of the formulation components, leading to a decrease in drug stability over time. Therefore, maintaining a lower storage temperature is crucial to preserving the integrity and stability of the PTX/AgNPs and HA/PTX/ AGNPs formulations. The results from stability testing revealed that the formulation stored at 4±2°C exhibited higher stability compared to those stored at 25±2°C. These findings suggest that storing AgNPs formulations in at 4±2°C is advisable to maintain their stability and integrity over time.

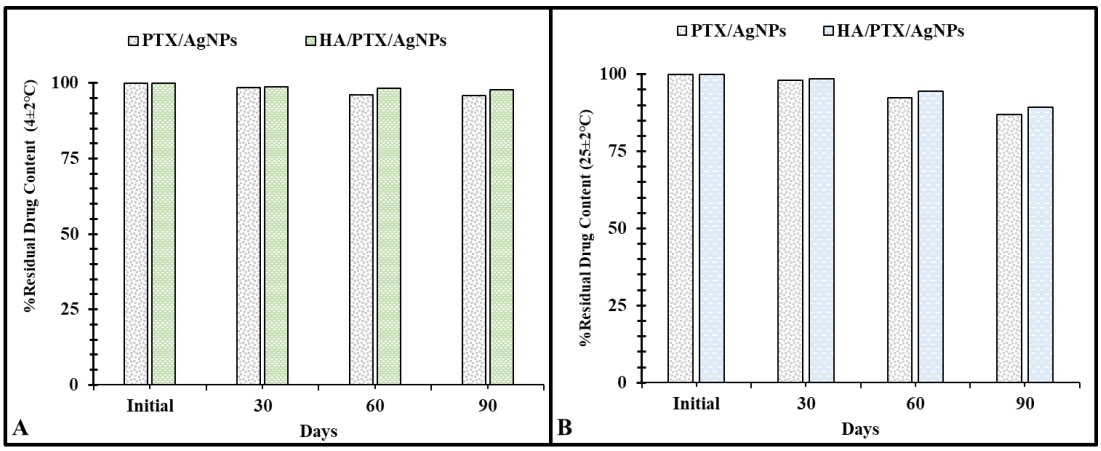

Figure 9: % Residual Drug Content after storage at (A) 4±1°C (B) 25±2°C

Conclusion

The main objective of this study was to develop and investigate the potential of AgNPs as a delivery system for the anticancer drug, paclitaxel (PTX). To achieve this, PTX-loaded AgNPs and HA/AgNPs were synthesized using turmeric extract through an environmentally friendly approach. Three different formulations with varying concentrations of $AgNO_3$ (1.0 mM, 1.5 mM, and 2.0 mM) were prepared. The formulation with an optimized concentration of 1.5 mM of silver nitrate demonstrated the best results in terms of particle size and drug entrapment efficiency. Further characterization of the optimized formulation was conducted

using FTIR, DSC, and XRD techniques. The drug release study confirmed a sustained release effect in the optimized formulation.

Acknowledgement

Authors are highly thankful to HIMT College of Pharmacy, Greater Noida, UP, India for providing facilities to complete this Project.

Conflict of interest

None

References

Alsammarraie, F. K., Wang, W., Zhou, P., Mustapha, A., & Lin, M. (2018). Green synthesis of silver nanoparticles using turmeric extracts and investigation of their antibacterial activities. *Colloids and Surfaces B: Biointerfaces*, *171*, 398-405.

Ashique S, Garg A, Mishra N, Raina N, Ming LC, Tulli HS, Behl T, Rani R, Gupta M. Nano-mediated strategy for targeting and treatment of non-small cell lung cancer (NSCLC). Naunyn-Schmiedeberg's Archives of Pharmacology. 2023 May 23:1-24.

Blackadar, C. B. (2016). Historical review of the causes of cancer. *World journal of clinical oncology*, *7*(1), 54.

Cruz, C. S. D., Tanoue, L. T., & Matthay, R. A. (2011). Lung cancer: epidemiology, etiology, and prevention. *Clinics in chest medicine*, *32*(4), 605-644.

Desai AS, Ashok A, Edis Z, Bloukh SH, Gaikwad M, Patil R, Pandey B, Bhagat N. Meta-Analysis of Cytotoxicity Studies Using Machine Learning Models on Physical Properties of Plant Extract-Derived Silver Nanoparticles. International Journal of Molecular Sciences. 2023 Feb 20;24(4):4220.

Ezhilarasan, D., Lakshmi, T., & Mallineni, S. K. (2022). Nano-based targeted drug delivery for lung cancer: therapeutic avenues and challenges. *Nanomedicine*, *17*(24), 1855-1869.

Ferreres, G., Pérez-Rafael, S., Torrent-Burgués, J., & Tzanov, T. (2021). Hyaluronic acid derivative molecular weight-dependent synthesis and antimicrobial effect of hybrid silver nanoparticles. *International journal of molecular sciences*, *22*(24), 13428.

Giubertoni, G., Koenderink, G. H., & Bakker, H. J. (2019). Direct observation of intrachain hydrogen bonds in aqueous hyaluronan. *The Journal of Physical Chemistry A*, *123*(38), 8220-8225.

Gomes, H. I., Martins, C. S., & Prior, J. A. (2021). Silver nanoparticles as carriers of anticancer drugs for efficient target treatment of cancer cells. *Nanomaterials*, *11*(4), 964.

Goudarzi, M., Mir, N., Mousavi-Kamazani, M., Bagheri, S., & Salavati-Niasari, M. (2016). Biosynthesis and characterization of silver nanoparticles prepared from two novel natural precursors by facile thermal decomposition methods. *Scientific reports*, *6*(1), 32539.

Hanahan, D. (2022). Hallmarks of cancer: new dimensions. *Cancer discovery*, *12*(1), 31-46.

Haque, M. N., Kwon, S., & Cho, D. (2017). Formation and stability study of silver nano-particles in aqueous and organic medium. *Korean Journal of Chemical Engineering*, *34*, 2072-2078.

Islami, F., Goding Sauer, A., Miller, K. D., Siegel, R. L., Fedewa, S. A., Jacobs, E. J., ... & Jemal, A. (2018). Proportion and number of cancer cases and deaths attributable to potentially modifiable risk factors in the United States. *CA: a cancer journal for clinicians*, *68*(1), 31-54.

Luo, Y., Cai, X., Li, H., Lin, Y., & Du, D. (2016). Hyaluronic acid-modified multifunctional Q-graphene for targeted killing of drug-resistant lung cancer cells. *ACS applied materials & interfaces*, *8*(6), 4048-4055.

Mavaei, M., Chahardoli, A., Shokoohinia, Y., Khoshroo, A., & Fattahi, A. (2020). One-step synthesized silver nanoparticles using isoimperatorin: evaluation of photocatalytic, and electrochemical activities. *Scientific reports*, *10*(1), 1762.

Prajapati, S. K., Jain, A., Jain, A., & Jain, S. (2019). Biodegradable polymers and constructs: A novel approach in drug delivery. *European polymer journal*, *120*, 109191.

Rajendran R, Pullani S, Thavamurugan S, Radhika R, Lakshmi Prabha A. Green fabrication of silver nanoparticles from Salvia species extracts: characterization and anticancer activities against A549 human lung cancer cell line. Applied Nanoscience. 2023 Mar;13(3):2571-84.

Rajput, S., Kumar, D., & Agrawal, V. (2020). Green synthesis of silver nanoparticles using Indian Belladonna extract and their potential antioxidant, anti-inflammatory, anticancer and larvicidal activities. *Plant cell reports*, *39*(7), 921–939.

Stino, S. (2022). Thermal analysis of dental materials: Differential Thermal Analysis (DTA)-Differential Scanning Calorimetry (DSC)-Thermogravimetric Analysis (TGA). *Biomaterials Journal*, *1*(12), 15-23.